Direction Finding and Likelihood Ratio Detection for Oceanographic HF Radars

BRIAN EMERY,[a] ANTHONY KIRINCICH,[b] AND LIBE WASHBURN[a,c]

[a] *Marine Science Institute, University of California, Santa Barbara, Santa Barbara, California*
[b] *Woods Hole Oceanographic Institution, Woods Hole, Massachusetts*
[c] *Department of Geography, University of California, Santa Barbara, Santa Barbara, California*

(Manuscript received 19 August 2021, In final form 3 November 2021)

ABSTRACT: Previous work with simulations of oceanographic high-frequency (HF) radars has identified possible improvements when using maximum likelihood estimation (MLE) for direction of arrival; however, methods for determining the number of emitters (here defined as spatially distinct patches of the ocean surface) have not realized these improvements. Here we describe and evaluate the use of the likelihood ratio (LR) for emitter detection, demonstrating its application to oceanographic HF radar data. The combined detection–estimation methods MLE-LR are compared with multiple signal classification method (MUSIC) and MUSIC parameters for SeaSonde HF radars, along with a method developed for 8-channel systems known as MUSIC-Highest. Results show that the use of MLE-LR produces similar accuracy, in terms of the RMS difference and correlation coefficients squared, as previous methods. We demonstrate that improved accuracy can be obtained for both methods, at the cost of fewer velocity observations and decreased spatial coverage. For SeaSondes, accuracy improvements are obtained with less commonly used parameter sets. The MLE-LR is shown to be able to resolve simultaneous closely spaced emitters, which has the potential to improve observations obtained by HF radars operating in complex current environments.

SIGNIFICANCE STATEMENT: We identify and test a method based on the likelihood ratio (LR) for determining the number of signal sources in observations subject to direction finding with maximum likelihood estimation (MLE). Direction-finding methods are used in broad-ranging applications that include radar, sonar, and wireless communication. Previous work suggests accuracy improvements when using MLE, but suitable methods for determining the number of simultaneous signal sources are not well known. Our work shows that the LR, when combined with MLE, performs at least as well as alternative methods when applied to oceanographic high-frequency (HF) radars. In some situations, MLE and LR obtain superior resolution, where resolution is defined as the ability to distinguish closely spaced signal sources.

KEYWORDS: Ocean; Algorithms; Data quality control; Radars/radar observations; Remote sensing; Surface observations; Quality assurance/control

1. Introduction

In the last 20 years significant effort and expense have been directed toward the construction of networks of oceanographic high-frequency (HF) radars. These radars primarily measure the coastal ocean surface current, though waves and winds are also possible products (Wyatt et al. 2006; Kirincich 2016). Each of these data products relies on signal-processing methods to extract the variable of interest and place it in space, typically through the application of direction-of-arrival (DOA) methods.

Oceanographic HF radars employ general-purpose DOA methods developed for diverse applications including radar and sonar. A review of the signal-processing literature indicates many advances in DOA methods over the last few decades (Krim and Viberg 1996). Much of our recent efforts have been geared toward revisiting these methods, with the overall goal of improving the observational capabilities of HF radars.

Our previous work in this field has identified and assessed alternative DOA methods, while uncovering new problems in their application. Emery (2020) used simulations to evaluate five DOA methods, including the commonly used multiple signal classification method (MUSIC; Schmidt 1986), finding the most improvement when using maximum likelihood estimation (MLE; Ziskind and Wax 1988). This study, combined with the results of Kirincich et al. (2019), illustrate the interdependence of DOA and the algorithm for determining of the number of simultaneous signal source bearings in producing low-error radial component data. In the signal-processing literature, these algorithms are known as "detection" methods (cf. Wax and Kailath 1985; Wax 1991).

Kirincich et al. (2019) used several different methods for detection, along with several of the most promising DOA methods, applying these to data obtained from University of Hawai'i High Frequency Doppler Radars (UH-HFDR; known colloquially as LERA). These systems are deployed within the Martha's Vineyard Coastal Observatory, with the receive antennas arranged on a square grid (diagonal distance equal to 1 radar wavelength). Receive antennas are located at all but one of the grid locations producing an 8-element receive array (referred to here as an RA-8 arrangement). Detection methods employed by Kirincich et al. (2019) include the Akaike information criterion (AIC), the minimum

Corresponding author: Brian Emery, brian.emery@ucsb.edu

DOI: 10.1175/JTECH-D-21-0110.1

descriptive length (MDL) (both described by Wax and Kailath 1985), a generalization of the Barrick and Lipa (1999) method to $M > 3$-element arrays (where M is the number of receive antennas), and an empirical method first described in Laws et al. (2000) and referred to as MUSIC-Highest. MUSIC-Highest is based on the relationship between the number of simultaneous signal source bearings (defined here as N) and the number of peaks in the MUSIC spectrum. The study found the best performance when using MUSIC for DOA with MUSIC-Highest for detection.

Each of the detection methods used by Kirincich et al. (2019) employ properties of the eigenvalues of the data covariance matrix $\mathbf{C}$. Typically, $\mathbf{C}$ is formed from the complex antenna voltage time series; however, in oceanographic HF radar, these have been filtered by two applications of the FFT, first to separate the signals by range, and second to separate them by Doppler velocity, such that $\mathbf{C}$ is formed for each range-Doppler bin separately. With the exception of MUSIC-Highest, these detection methods assume a clear break in the eigenvalues, which can be used to partition the signal and noise, with the noise eigenvalues having roughly equal value. In many signal-processing situations, such as a strong signal in white Gaussian noise, this will be a valid assumption. However, evidence suggests that this scenario does not include ocean backscatter at HF. For example, Fig. 1 below, as well as Fig. 8 of Kirincich et al. (2019), show a linear drop in magnitude, rather than a break between signal and equal-valued noise. While the method of Barrick and Lipa (1999) and MUSIC-Highest use additional information to improve their detection capabilities, other studies indicate limitations inherent to any DOA method based on the eigendecomposition.

Example limitations of DOA methods using eigendecomposition include restrictions on resolution and poor performance when the signal-to-noise ratio (SNR) is low. Defining resolution as the ability to distinguish between closely spaced signal sources, Tuncer et al. (2009) citing Amar and Weiss (2007) suggest a theoretical limit on the minimum separation achievable by MUSIC, as a function of the receive array beamwidth and the SNR. Ziskind and Wax (1988) suggest that the use of the full data covariance matrix, rather than components of the eigendecomposition, gives MLE an advantage in direction finding. While Kirincich et al. (2019) utilized MLE-based DOA methods, eigendecomposition-based methods were used for detection. Thus, a method for detection that is not based on the eigendecomposition is needed to realize any potential advantage of using MLE.

Previous publications suggest the use of the generalized likelihood ratio test (GLRT) for detection along with MLE for DOA. GLRT is based on a “goodness of fit” between a model of the data $\hat{\mathbf{C}}$ and $\mathbf{C}$ in the MLE calculation (Kelly and Forsythe 1989; Ottersten et al. 1993; Abramovich and Spencer 2004; Chandran 2006). In a typical application, the GLRT is used in a binary hypothesis test, determining the presence or absence of signal. In a later application, the GLRT philosophy is applied to the problem of determining N through the sequential calculation of the likelihood ratio (LR) (Chandran 2006; Abramovich et al. 2009). In the following we describe the LR calculation and apply it to oceanographic data, with the major objective of this paper being to evaluate the use of the LR with the MLE, and potentially, to realize improvements in HF radar data suggested by simulations in Emery (2020).

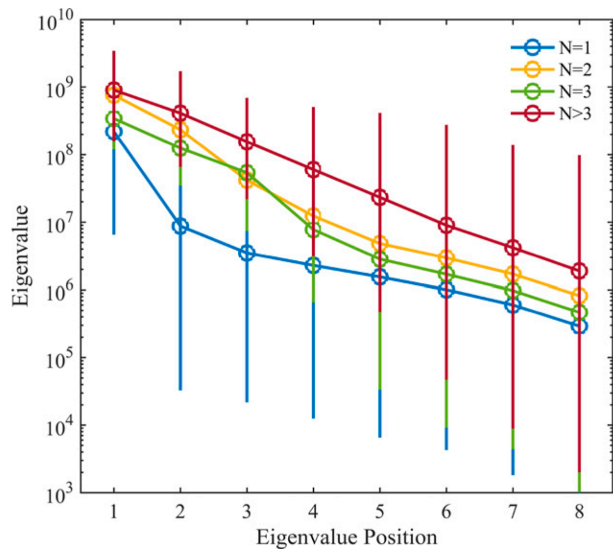

FIG. 1. Mean eigenvalues (with standard deviations) from simulated HF radar data for different flow conditions as quantified by the number of emitters N. The AIC and MDL criterion rely on a clear break between the signal and the noise eigenvalues—differences that are not often present in oceanographic HF radar data.

The remainder of the paper is organized as follows. In section 2 we briefly review HF radar processing including other detection methods typically used, present the LR calculation, and discuss the methods used for evaluating observations. Results of our analysis are presented in section 3, these are put into context with previous works in section 4, and our conclusions are presented in section 5.

2. Methods

a. Oceanographic HF radar signal processing

Here we briefly summarize signal-processing methods commonly used by oceanographic HF radars, as these have been described in detail elsewhere (cf. Lipa and Barrick 1983; de Paolo et al. 2007; Emery and Washburn 2019; Emery 2020). Oceanographic HF radars typically transmit radio waves swept over a range of frequencies, either interrupted briefly or not, which are then received and digitized. The frequency sweep associates frequency to range after FFT processing, and subsequent sweeps produce time series at a given range. The sweep typically spans tens or hundreds of kilohertz, whereas the Doppler information of interest is within ~1 Hz of the range equivalent frequency. A second, Doppler resolving FFT at a given range, then bins signals by Doppler velocity. For each Doppler frequency of interest, the auto- and cross-spectra are used to form a covariance matrix $\mathbf{C}$, specifying variance and covariance of the receive antennas. Since a single range cell may contain signal from several directions, the covariance matrix may contain signal from one to several directions if the same Doppler velocity occurs in these locations. The application of DOA methods to $\mathbf{C}$ determines the most likely source direction(s), allowing the known Doppler velocities to be localized on the ocean surface. Detection methods are used to specify which value of N is most valid.

Lipa and Barrick (1983) allude to the problem of detection for oceanographic radars, and Barrick and Lipa (1999) later provide a method for the 3-element SeaSonde. The SeaSonde detection method bases the decision between $N = 1$ and $N = 2$ on three criteria, including eigenvalue characteristics and characteristics of the signal power matrix. The method then compares the computed parameters with empirically determined thresholds to determine whether the $N = 1$ or $N = 2$ solution is most appropriate. For example, typical recommended values for the parameter set of [40 20 2] indicate that $N = 2$ when the ratio of the largest eigenvalue to the second largest is less than 40, the signal powers are within a factor of 20, and the product of the signal powers is more than a factor-of-2 larger than the product of the off-diagonal elements of the signal power matrix. Our implementation of this method (cf. Emery 2021) follows Barrick and Lipa (1999), and was used in processing SeaSonde data for this study. Note that this method can be considered an expansion upon the AIC and MDL techniques. We refer to the combination of direction finding with MUSIC and detection with the SeaSonde method as MUSIC-SS.

For the SeaSonde data, sets of 11 different detection parameters were used, as shown in Table 1. SeaSonde parameter sets were obtained by taking the three sets suggested by the manufacturer (CODAR Ocean Sensors, Ltd.) and interpolating/extrapolating over a wider range. LR threshold values ranged from 10 to 70 in increments of 5.

The MUSIC-Highest detection method described previously (Laws et al. 2000; Kirincich 2018; Kirincich et al. 2019) requires the number of distinct peaks in the MUSIC spectrum to match the dimension of the signal subspace N. Kirincich et al. (2019) applied peak thresholds of 0.05, 0.25, and 0.5 dB above background to distinguish peaks and found that the 0.5 dB was sufficient to remove spurious results and improve comparisons with drifters. For this study we allowed the threshold to vary from between 0.05 and 1.3 dB.

b. The likelihood ratio

Essentially, the LR calculation compares the data covariance obtained by the radar, with a model of the data formed from the DOA solution and receive antenna pattern. The LR calculation is performed jointly with the DOA calculation, for sequentially increasing values of N, up to $N < M$. The procedure for computing and applying the LR to oceanographic radar data was assembled from several sources as described below.

TABLE 1. Parameter sets used for detection with the SeaSonde method. Each rows denotes one set, with boldface font indicating the manufacturer-recommended options.

P1 (dB)	P2 (dB)	P3 (dB)
80	40	0
70	35	0.5
60	30	1
50	25	1.5
40	**20**	**2**
30	15	2.5
20	**10**	**3**
15	7.5	5.5
10	**5**	**8**
5	2.5	10.5
0	0	13

To compute the LR we first reconstruct an estimate of the data, defined as $\hat{\mathbf{C}}$,

$$\hat{\mathbf{C}} = \mathbf{ASA}^{\mathrm{H}} + \sigma\mathbf{I}, \qquad (1)$$

where $\mathbf{I}$ is the $M \times M$ identity matrix, H denotes the Hermitian transpose, $\mathbf{A}$ represents the $M \times N$ complex-valued antenna pattern at the N DOAs, given by $\mathbf{A}(\theta_N)$, σ is an estimate of the noise power, computed directly from the data by following the method of Ottersten et al. (1993):

$$\sigma = \frac{1}{M}\mathrm{Tr}\left[(\mathbf{I} - \mathbf{AA}^{\dagger})\mathbf{C}\right], \qquad (2)$$

where $\mathbf{A}^{\dagger}$ is the pseudoinverse of $\mathbf{A}$ [defined as $\mathbf{A}^{\dagger} = (\mathbf{A}^{\mathrm{H}}\mathbf{A})^{-1}\mathbf{A}^{\mathrm{H}}$], Tr is the matrix trace operator, and $\mathbf{C}$ is the data covariance matrix; $\mathbf{S}$ in (1) is the signal power matrix, also estimated from the data:

$$\mathbf{S} = \mathbf{A}^{\dagger}(\mathbf{C} - \sigma\mathbf{I})\mathbf{A}^{\dagger\mathrm{H}}. \qquad (3)$$

Having computed the data model $\hat{\mathbf{C}}$ for the N DOA solutions, we compute the LR:

$$\mathrm{LR} = -2\log\left(\left\{\frac{\det\left(\mathbf{C}\hat{\mathbf{C}}^{-1}\right)}{\left[\frac{1}{M}\mathrm{Tr}\left(\mathbf{C}\hat{\mathbf{C}}^{-1}\right)\right]^{M}}\right\}^{K}\right), \qquad (4)$$

where det is the matrix determinant and K is the number of data snapshots. Abramovich and Spencer (2004) and Abramovich et al. (2009) provide the argument to $-2\log()$ in (4), and Swindlehurst and Stoica (1998) suggest the $-2\log()$ transformation, which is useful given the very small values for the argument to $-2\log()$ that we obtain. Abramovich et al. (2009) specify the requirement that $K \geq M$, and several properties of the LR values, which we describe below. Other formulations for computing LR given by Ottersten et al. (1993), Swindlehurst and Stoica (1998), Chandran (2006), as well as an additional formulation in Abramovich et al. (2009), either do not have these properties, or the values we obtain do not conform to the properties they describe.

As defined in (4), the LR has several properties that enable its use in solving the detection problem. First, the range of LR values, and its probability density function (PDF), depend only on K and M, with a χ^2 distribution [Ottersten et al. (1993) citing Wilks (1938); Abramovich et al. (2009) states that the LR PDF is "scenario invariant" and independent of $\mathbf{C}$]. Second, minimum and maximum values for the LR can be found as follows. To find the minimum LR, set $\hat{\mathbf{C}} = \mathbf{C}$ in (4), which produces LR $= -2\log(1)$ or LR $= 0$, which would be the case of a perfect match between the data and the model. To find the maximum LR, set $\hat{\mathbf{C}} = \sigma\mathbf{I}$, which produces values of LR that become "large" (observations suggest a maximum of about 1500 with $K = 13$ and $M = 8$). Setting $\hat{\mathbf{C}} = \sigma\mathbf{I}$ is equivalent to modeling the data as uncorrelated noise (Ottersten et al. 1993), suggesting a poor match between the data and the model. The LR values computed with increasing values of N for a fixed $\mathbf{C}$ have a "nested property," where increasing N to produce $\hat{\mathbf{C}}$ results in decreasing values of the LR,

$$\mathrm{LR}_{N=1} \geq \mathrm{LR}_{N=2} \geq \cdots \geq \mathrm{LR}_{N}, \qquad (5)$$

assuming optimal DOA solutions (Chandran 2006). This property suggests the need to determine a threshold, below which the LR value indicates that the model–data fit is "good enough," and N is sufficient.

Given these properties of the LR, Abramovich et al. (2009) suggest using the LR for detection in a sequential procedure. For a given $\mathbf{C}$, start by forming $\hat{\mathbf{C}}$ for $N = 1$ and computing the LR, forming $\hat{\mathbf{C}}$ for $N = 2$, and so on, comparing the computed LR values with a threshold, and stopping once the threshold has been crossed. The lowest N that results in an LR value below the threshold is determined to be the number of emitters in the DOA solution. To determine appropriate thresholds for oceanographic HF data, we compare independent observations to identify and confirm threshold values as described below.

c. Calculation of the number of snapshots, K

Calculation of LR requires a known value for K, the number of data snapshots, or as defined by Van Trees (2002), the number of statistically independent intervals. For this study, our SeaSonde data processing averages six independent FFTs of 512 points each (256 s), from nonoverlapping Doppler spectra, spanning a total of 25.6 min. For covariance matrices derived from this processing we use $K = 6$. UH-HFDR systems used in this study produce averaged auto- and cross-spectra from overlapping segments, which complicates the calculation of K. These systems used 30 min time series segments sampled at 3.074 Hz, dividing these 5533 points into eight separate blocks of 2048 points each (e.g., with 78% overlap, or 1597 overlapping points). FFTs are computed after the application of the Hanning window to each segment. Following Percival et al. (1993) we estimate K by following methods for estimating the degrees of freedom for arbitrary window overlap. Using these parameters, the computed Doppler spectra have 16 degrees of freedom, suggesting $K = 8$ for the UH-HFDR observational data.

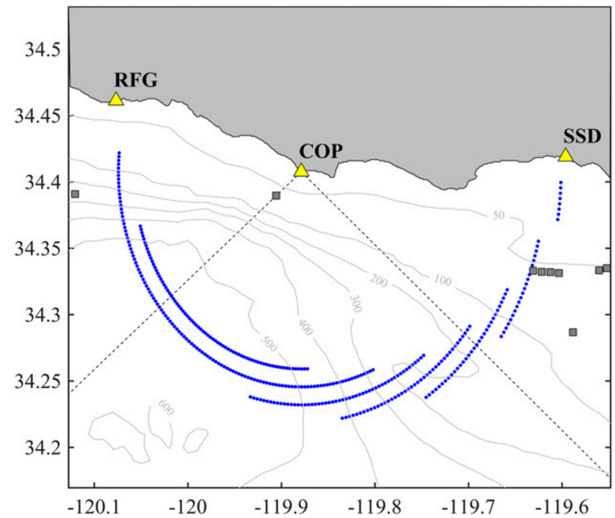

FIG. 2. Map of the vicinity of the Santa Barbara Channel showing the locations of HF radar sites used for computing synthetic radials from Refugio State Beach (RFG) and Summerland Sanitary District (SSD) (yellow triangles), and the grid used for total vector calculations (blue dots) for comparison with data from the HF radar at Coal Oil Point (COP). Gray squares show oil production platforms, dashed lines show bearings 219° and 320° from COP (counterclockwise from east), and bathymetry is in meters.

d. SeaSondes and synthetic radial comparisons

To provide independent observations with spatially similar resolution for method and threshold validation, we extend the method for comparing radar observations along overwater baselines (Lipa 2003; Lipa et al. 2006; Paduan et al. 2006), to regions where overwater baselines do not exist. This approach uses data from multiple radars to estimate the radial component at an additional radar (cf. Kirincich et al. 2019). Independent estimates of the radial components synthesized from other radars, defined as synthetic radials, requires having multiple radars observing the same area of the sea surface from different locations. Figure 2 shows an example grid located on the ocean surface that is within the view of three SeaSonde HF radars. Each grid point obtains orthogonal observations from the two outer HF radars [located at Refugio State Beach (RFG), California, and the Summerland Sanitary District (SSD), California]. We first compute total vectors from RFG and SSD (Kaplan et al. 2007), and then estimate the radial velocity component $\mathbf{v}_r$ at Coal Oil Point (COP), California, such that the comparisons cover similar spatial extents over similar time intervals. This method provides a wide range of bearings where independent estimates of $\mathbf{v}_r$ can be compared while avoiding some of the differences inherent when comparing HF radars with in situ observations.

In this study, the time series spanning 0000 UTC 1 October–2230 UTC 25 October 2017 was processed with both MLE-LR and MUSIC-SS, with LR and SS parameters allowed to vary over the full range of values as described above. We base comparison statistics on observations from a bearing-limited region (relative to COP) given by 219°–320° (dashed lines Fig. 2) to

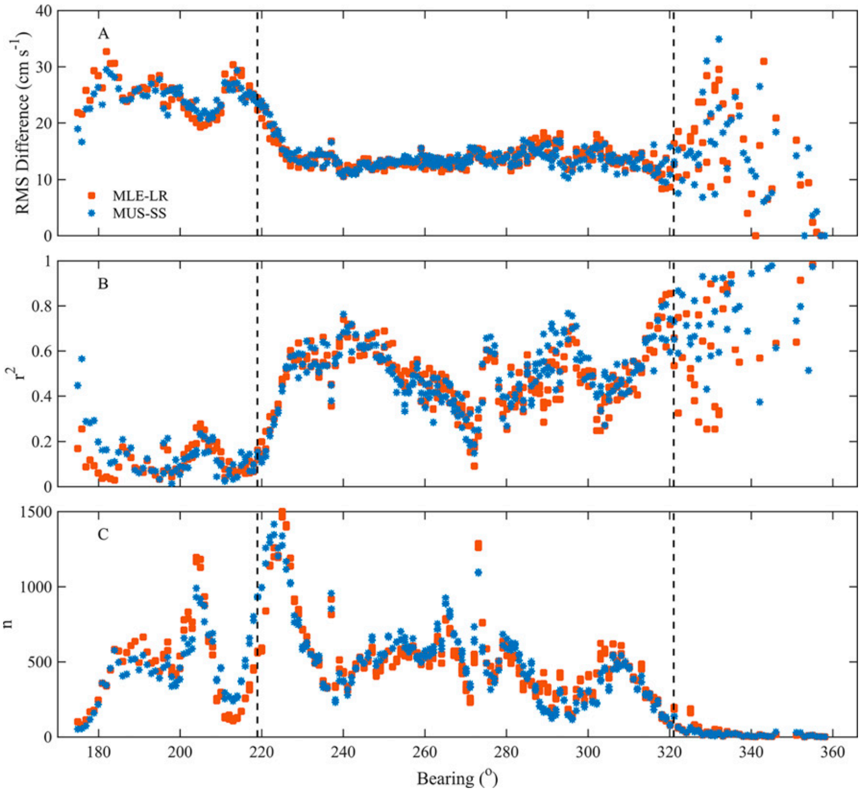

FIG. 3. Comparisons between radial surface currents from RFG-SSD and COP, as a function of bearing, for the two detection–estimation methods (MLE-LR and MUSIC-SeaSonde), with LR = 70 and the SeaSonde parameter set [0 0 13]: (a) RMS difference σ_{RMS}, (b) r^2, and (c) the number of radial velocity observations n used to compute σ_{RMS} in (a) at each location. The vertical dashed lines are located at bearings of 219° and 320° as in Fig. 2.

reduce influence of significant radio-wave propagation across land for SSD, and the influence of an oil production platform (located 3.2 km along bearing 219° from COP) for both RFG and COP.

e. UH-HFDR and drifter observations

The UH-HFDR systems were located at the Long Point Wildlife Refuge on Martha's Vineyard, Massachusetts (designated as LPWR), and the Nantucket Wastewater Treatment Plant on Nantucket Island, Massachusetts (designated as NWTP) (Kirincich et al. 2019). Performance of the DOA estimation and detection methods used with these systems are assessed with data from a mass drifter release conducted in August of 2018. The drifter release (and deployment of LPWR) were conducted as part of an NSF-funded study of the inner shelf off Martha's Vineyard. During 14–22 August 2018, the release of 24 CODE–style surface drifters (Davis 1985), occurred within the LPWR coverage area, and slightly to the west of the main NWTP coverage area. The LPWR and NWTP radars operated at 16.1 and 16.2 MHz, respectively, such that the 0.75-m effective depth of the HF radar measurement (Stewart and Joy 1974) roughly corresponds to the 1-m maximum drogue depth. After binning the drifter data in time (~30 min) and space (1° by 2 km) to coincide with the radar observations, several hundred data points are available for comparison over the eight days of overlapping drifter–radar observations.

3. Results

a. SeaSonde observations: Synthetic radial comparisons

Figure 3 shows σ_{RMS}, correlation coefficient squared r^2, and the number of observations n between the RFG–SSD synthetic radials and COP radials for both MUSIC-SS and MLE-LR, plotted as a function of bearing relative to COP. To produce this figure, data from all three SeaSondes were processed using 70 as the LR threshold and [0 0 13] as the SeaSonde parameter set. For both methods, high σ_{RMS}, low r^2, and low n are found for bearings outside the range 219°–320°. Within 219°–320°, results for both methods are similar, with consistent σ_{RMS}, and variable r^2. Figure 3b results suggest that some bearings produce noisier current observations than others. Results for r^2 are also somewhat inversely related to n used in the calculation. Overall, the results with the SeaSonde observations show similar performance

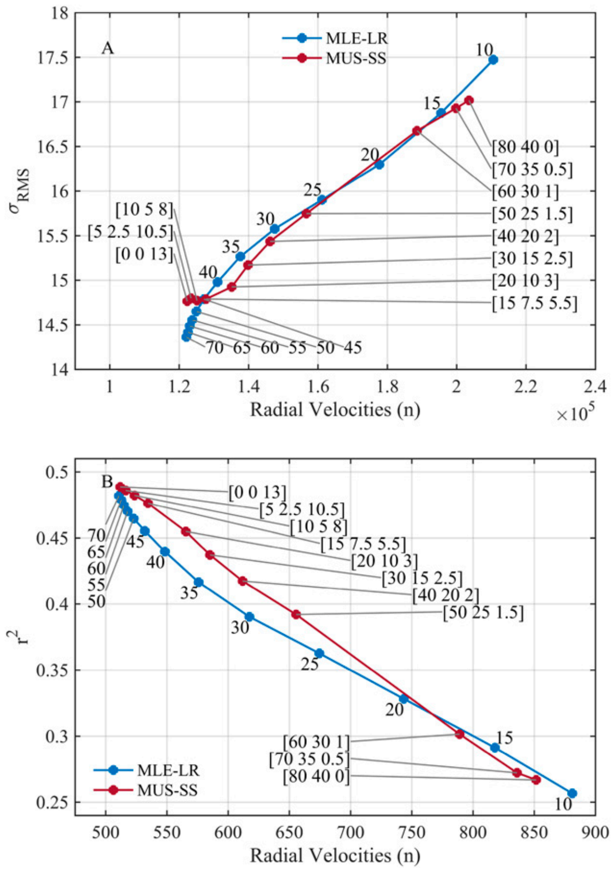

FIG. 4. Comparisons between COP radials and synthetic radials generated from RFG-SSD, in the bearing-limited region of Fig. 2, for varying detection parameters (LR and SeaSonde): (a) $\sigma_{\rm RMS}$ vs n and (b) r^2 vs n. In (b) r^2 is computed for each grid location over the month-long time series and then averaged spatially such that (b) shows the spatially averaged r^2 vs spatially averaged n for each of the comparison datasets.

for both DOA–detection methods for these detection parameters.

Figure 4 provides aggregate results of the synthetic radial comparisons, in terms of $\sigma_{\rm RMS}$ and r^2, for each of the different detection parameters used (both LR and SS). Calculations for this figure use observations obtained on the grid between bearings 219° and 320° (Fig. 2), with Fig. 4a showing the RMS difference versus the number of radial velocity observations n. Figure 4b shows the spatially averaged r^2 versus spatially average n, where r^2 is computed for each grid location over the month-long time series as in Fig. 3, and then averaged between bearings 219° and 320° to produce the values shown. The results show similar overall $\sigma_{\rm RMS}$ and r^2 between the methods, with minimum values (~15 cm s^{-1}) on the upper end typical of previous HF radar comparisons, and r^2 values on the low end (cf. Graber et al. 1997; Emery et al. 2004; Ohlmann et al. 2007; Molcard et al. 2009; Liu et al. 2010; Cosoli et al. 2010). The lowest $\sigma_{\rm RMS}$ is obtained with MLE-LR. Both methods produce improved comparisons when detection parameters result in more $N = 1$ solutions, which results in fewer radials (n) for comparison. Taking the MLE-LR results for example, the lowest n corresponds with the lowest $\sigma_{\rm RMS}$ and highest r^2. These results occur when the LR threshold is set to 70. With the threshold at 70, 90% of the solutions are $N = 1$ solutions—so-called single-bearing solutions. Similarly, SeaSonde parameters that select for more single-bearing solutions produce the best comparison statistics, with the three most stringent selecting for 96%, 98%, and 100% single-bearing solutions at roughly the same $\sigma_{\rm RMS} = 14.8$ cm s^{-1} and $r^2 = 0.49$. In comparison, the widely used SeaSonde parameter set [40 20 2] obtains $\sigma_{\rm RMS} = 15.4$ cm s^{-1} and $r^2 = 0.42$, with 68% single-bearings solutions. Overall, note that the approximately 65% increase in n corresponds to 15% increase in $\sigma_{\rm RMS}$.

b. UH-HFDR observations: Drifter comparisons

Figure 5 shows comparison statistics $\sigma_{\rm RMS}$ and r^2 versus n for variable detection thresholds, both LR and MUSIC-Highest. The overall results for the two radar sites somewhat contradict each other, with MLE-LR producing the best comparisons at NWTP, and MUSIC-Highest producing the best comparisons at LPWR. Furthermore, MLE-LR results from NWTP suggest a trade-off between more observations (n) and diminished comparison statistics, as found with the SeaSonde results (Fig. 4), while MUSIC-Highest at NWTP along with both methods at LPWR show little relation between statistics and n for variable threshold parameters. For both sites and both DOA–detection methods, the best comparisons are found with thresholds that favor lower values of N, which we discuss further below.

Figure 6 and Table 2 show the results of drifter–radar comparisons for the two HF radars, with the LR threshold set to 800 and the MUSIC-Highest threshold set to 1.3, respectively. The decreased performance for MUSIC-Highest for NWTP (Figs. 6a,b) seems to result from a small number of outliers, while MLE-LR performs well, though obtaining slightly fewer observations. Figures 6c and 6d show results for LPWR, with superior performance for MUSIC-Highest, and increased observations away from the 1:1 line for MLE-LR, resulting in lower r^2 and higher $\sigma_{\rm RMS}$ from about 7% more observations. To better illustrate the relative performance of the two DOA–detection methods, Fig. 7 and Table 3 show the comparison data only when observations are present simultaneously for both radar DOA–detection methods and the drifters. These comparisons suggest similar accuracy when using MLE-LR for NWTP, and significantly improved accuracy when using MUSIC-Highest at LPWR.

4. Discussion

a. Comparison with previous studies

The simulation-based study by Emery and Washburn (2019) provides a look at DOA performance independent of detection methods, by obtaining the value of N used by the DOA algorithms from the input flow field. The study suggests

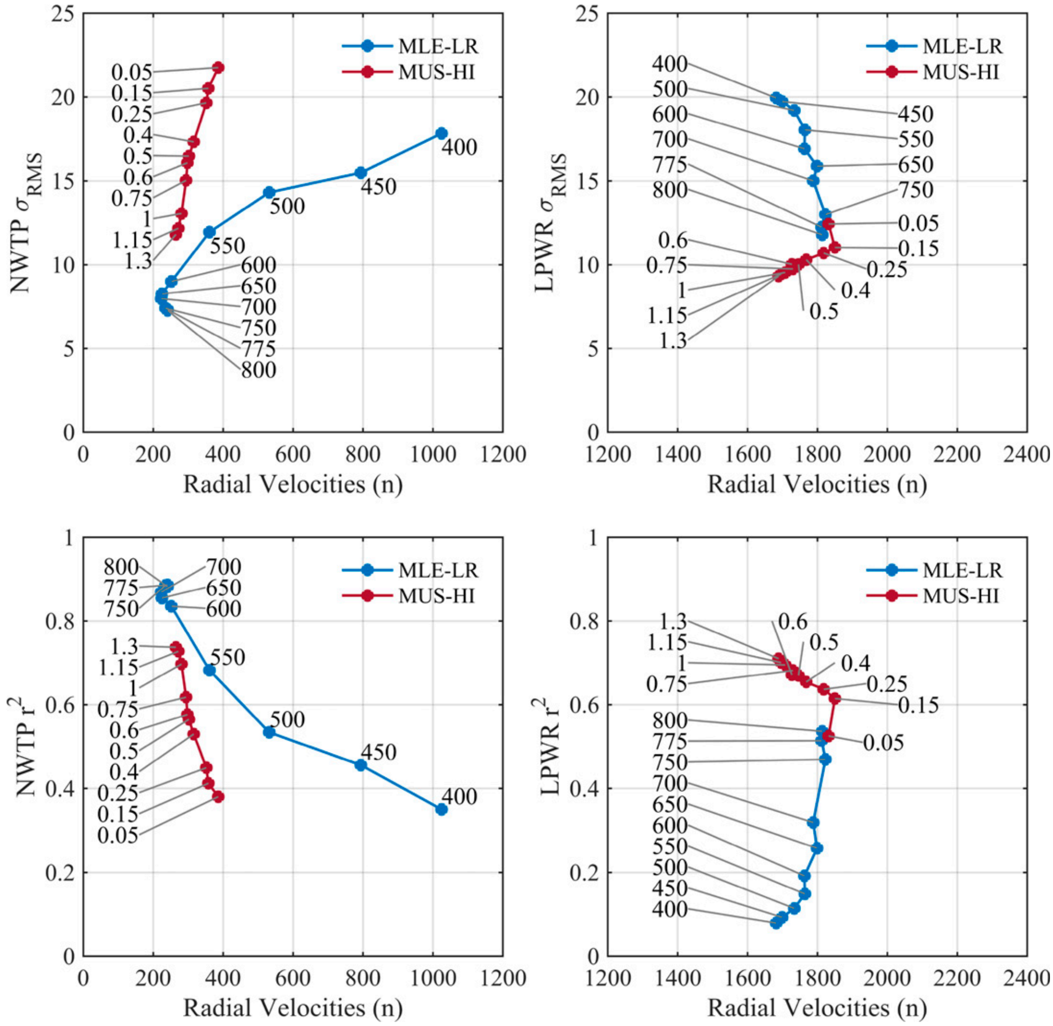

FIG. 5. Comparison statistics of UH-HFDR data vs drifters for varying detection parameters (LR and MUSIC-Highest). (left) NWTP vs drifters and (right) LPWR vs drifters for (top) σ_{RMS} vs n and (bottom) r^2 vs n.

similar performance between DOA methods for SeaSondes in terms of the accuracy of the observations, with potential improvements for MLE in terms of the n returned, that is, in terms of the percent coverage resulting from increased numbers of $N = 2$ solutions. Results here however show that depending on the threshold criteria, improvements in coverage can be had for both methods, though these come with increased σ_{RMS} and lower r^2 (Fig. 4). Simulations in Emery and Washburn (2019) suggest that 20%–50% increases in n can be associated with relatively small changes in comparison statistics. Figure 4a similarly suggests that up to a 70% increase in coverage (as shown by n) can be had at the cost of an approximately 15% increase in RMS difference and 45% decrease in r^2.

For RA-8 arrays, Emery and Washburn (2019) suggest some improvement in accuracy with the use of MLE, along with significant improvements in coverage relative to MUSIC. However, comparisons here between drifters and the RA-8 array radars at NWTP and LPWR found mixed results. Increased accuracy with slightly fewer comparisons was found by using MLE-LR at NWTP. Similar accuracy can also be had, with an increase in n for MLE (e.g., with LR = 550 and MUSIC-Highest set to 1.15). Comparisons at LPWR found the opposite result (Fig. 5) with the best comparisons found for MUSIC-Highest. At the total vector level, the extreme values for detection parameters (e.g., LR = 400) used with the UH-HFDR systems do increase coverage. However, the resulting total vector maps are qualitatively noisier and, in several instances, produce realistic-looking flow features that our analysis strongly suggests are not real. Because of these flow features, we would not recommend the use of the more extreme detection parameters (e.g., LR $\leq$ 600 or MUSIC-Highest $\leq$ 0.4).

While a lack of appropriate observations precludes a direct comparison of the relative performance of the SeaSonde versus UH-HFDR systems, a comparison with previously published statistics is possible. Kirincich et al. (2019) performed synthetic radial comparisons on the UH-HFDR observations made at NWTP, using two adjacent SeaSondes,

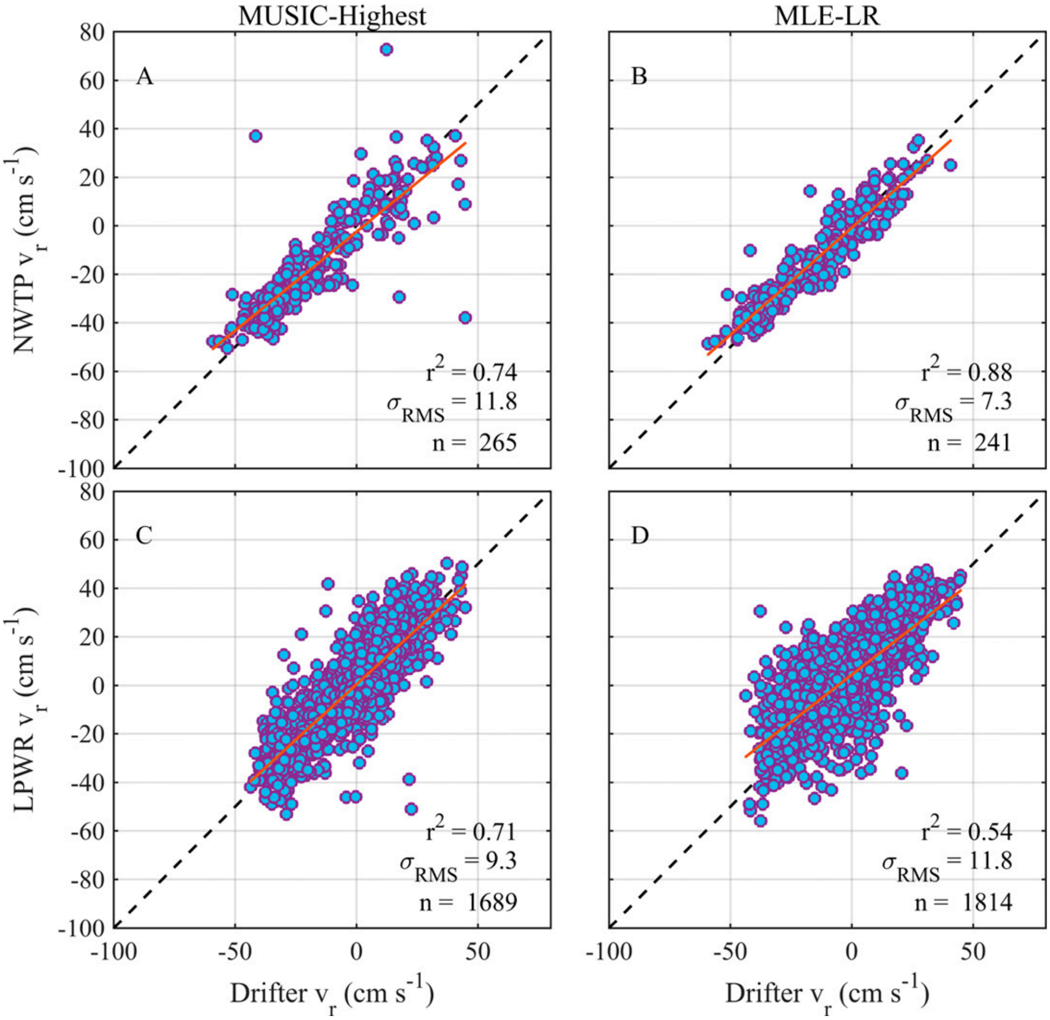

FIG. 6. Scatterplots of UH-HFDR data vs drifters. (top) NWTP vs drifters, radar processed with (a) MUSIC-Highest (set to 1.3) and (b) MLE-LR (set to 800). (bottom) LPWR vs drifters, radar processed with (c) MUSIC-Highest and (d) MLE-LR (showing only data east of 240° bearing for LPWR). The least squares fit line is shown in red (see Table 2).

finding RMS differences in the range 10–15 cm s^{-1} and r^2 in the range 0.74–0.83. These results are slightly lower than the radar-to-radar comparisons found for the Santa Barbara Channel SeaSondes, with best RMS differences near 14.5 cm s^{-1} and r^2 near 0.49.

b. DOA resolution

Tuncer et al. (2009) suggests a DOA performance metric defined as the ability to resolve two or more closely spaced signals, when considering signals present in the same covariance matrix (i.e., the same Doppler velocity). For this definition of resolution, the minimum value for MUSIC can be estimated in terms of the beamwidth (BW) in degrees and the SNR:

$$\delta\theta = \frac{\mathrm{BW}}{\mathrm{SNR}^{(1/2)}} \tag{6}$$

(Amar and Weiss 2007). Here $\delta\theta$ gives the minimum separation between signal sources that MUSIC can resolve at the

TABLE 2. Statistics of UH-HFDR-vs-drifter comparisons over 14–22 Aug 2018, as quantified by the correlation coefficient squared (r^2), the root-mean-square difference (RMS diff), mean absolute error (MAE), and slope and intersect of the least squares fit line.

Site	Methods	r^2	RMS diff (cm s^{-1})	MAE (cm s^{-1})	Slope	Intercept	Obs
NWTP	MUSIC-Highest	0.74	11.8	7.2	0.8	−2.5	265
NWTP	MLE-LR	0.88	7.3	5.5	0.9	−0.9	241
LPWR	MUSIC-Highest	0.71	9.3	6.7	0.9	0.4	1689
LPWR	MLE-LR	0.54	11.8	8.9	0.8	4.3	1814

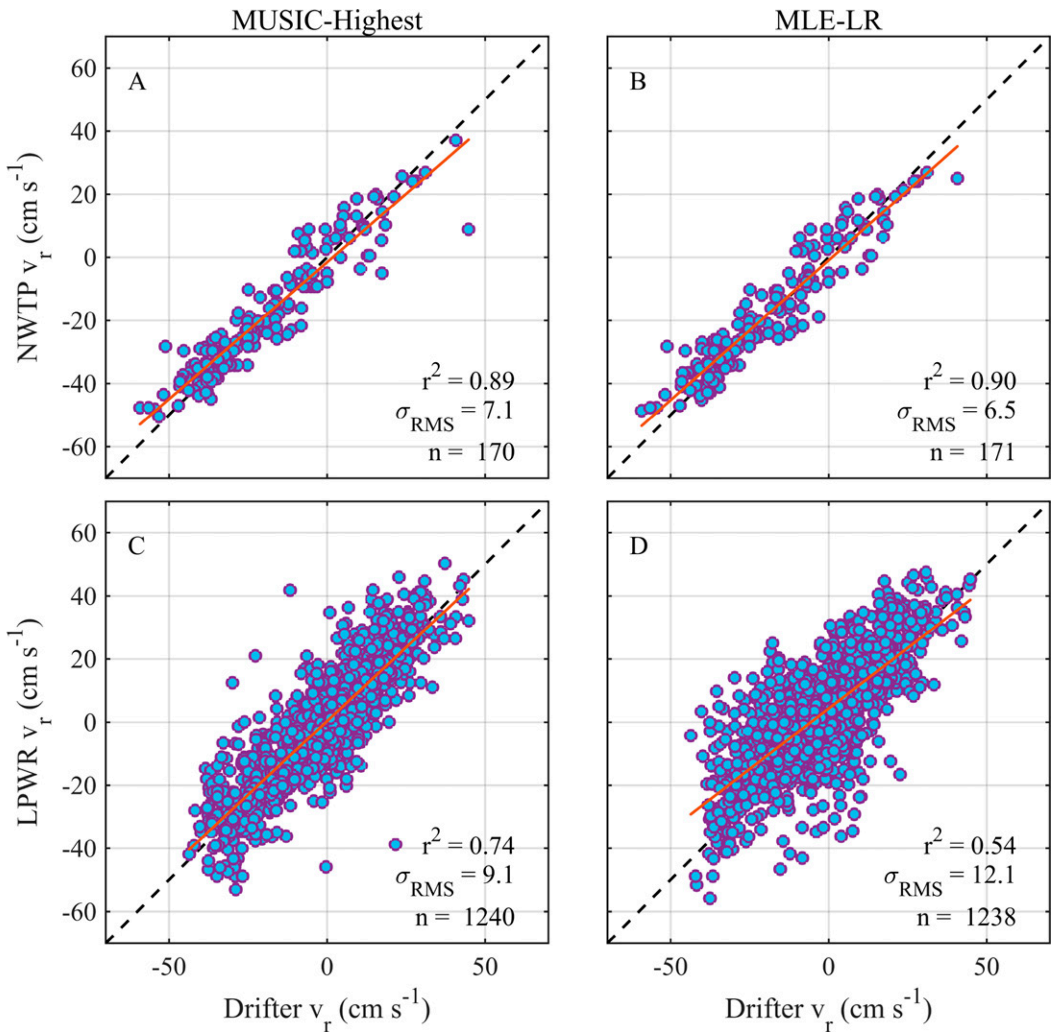

FIG. 7. Scatterplots of UH-HFDR data vs drifters, for times when observations are present simultaneously for the drifters and both radar DOA–detection methods. (top) NWTP vs drifters, radar processed with (a) MUSIC-Highest and (b) MLE-LR. (bottom) LPWR vs drifters, radar processed with (c) MUSIC-Highest and (d) MLE-LR (showing only data east of 240° bearing for LPWR).

given SNR. Applying this theory to the SeaSonde and RA-8 receive arrays suggests minimum separation for MUSIC of about 24° and 9°, respectively (both at 30-dB SNR, using 131° beamwidth for the SeaSonde and 49° for the RA-8; Van Trees 2002). Using our observations, we compute $\delta\theta$ for the systems at COP and LPWR for MUSIC and MLE DOA methods. Figure 8 shows histograms of the separation in degrees between DOA solutions from the same covariance matrix when $N > 1$ for the sites COP and LPWR. The COP SeaSonde data shown here used LR = 25 and [50 25 1.5] for detection, while data from LPWR used LR = 800 and MUSIC-Highest 1.3 for detection. Figures 8a and 8b show that the SeaSonde at COP obtained two-bearing solutions with separations less than 24° for about 15% of two-bearing solutions for MUSIC-SS, while MLE-LR found separations less than 24° for about 38% of the two-bearing solutions.

TABLE 3. As in Table 2, but based only on observations coincident to both DOA–detection methods and the drifters.

Site	Methods	r^2	RMS diff (cm s^{-1})	MAE (cm s^{-1})	Slope	Intercept	Data points
NWTP	MUSIC-Highest	0.89	7.1	5.2	0.9	−1.6	170
NWTP	MLE-LR	0.90	6.5	5.0	0.9	−1.0	171
LPWR	MUSIC-Highest	0.74	9.1	6.6	0.9	0.3	1240
LPWR	MLE-LR	0.54	12.1	9.2	0.8	4.3	1238

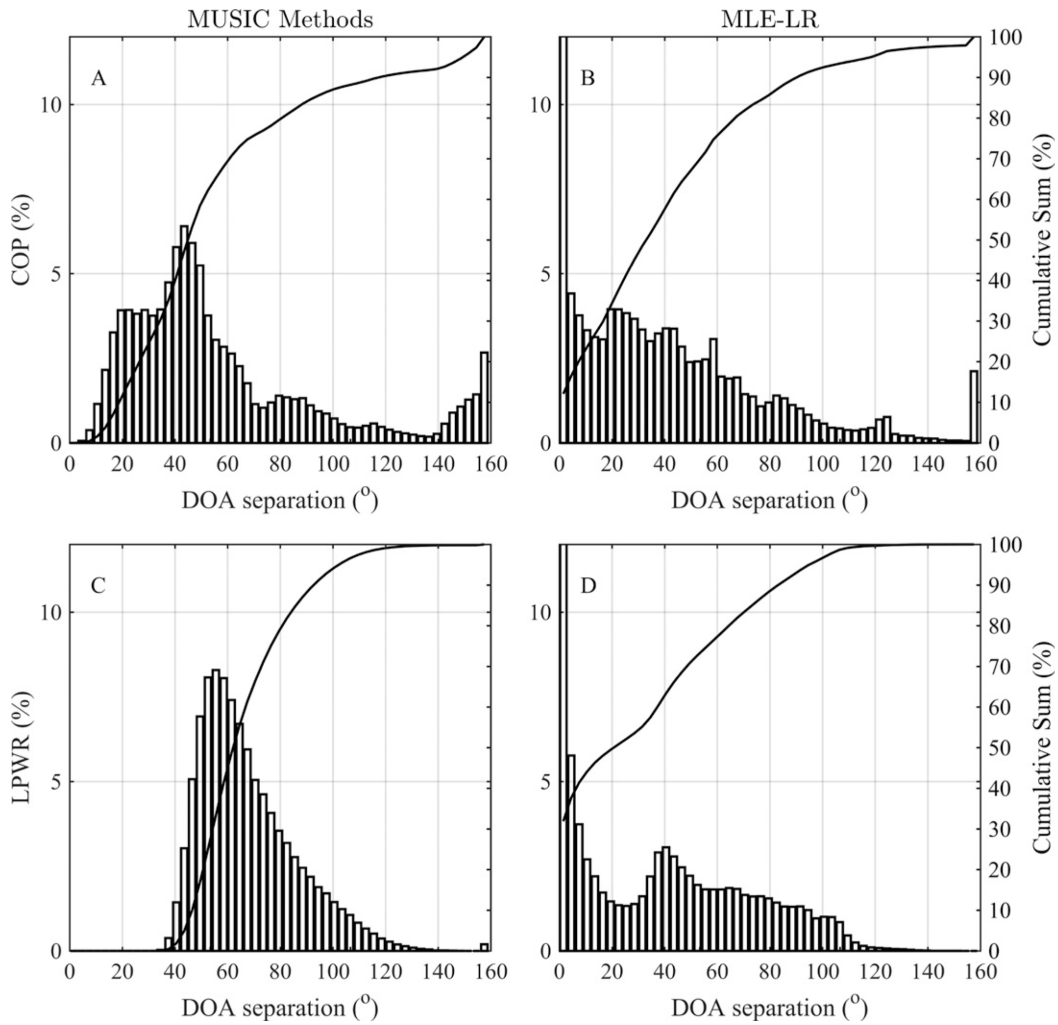

FIG. 8. Histograms of separation (°) between DOA solutions from individual covariance matrices (a) from COP with MUSIC-SS, (b) from COP with MLE-LR (the maximum of the first bin is 12.0%, which can be obtained from the first point on the cumulative sum curve), (c) from LPWR with MUSIC-Highest, and (d) from LPWR with MLE-LR (the maximum of the first bin is 31.9%).

Results for LPWR are shown in Figs. 8c and 8d, with minimum separations for MUSIC-Highest near 34.5°, well above the predicted value of 9°. MLE-LR found separations less than 9° for about 41% of the $N > 1$ solutions (and separations less than 34.5° occurring for about 57%). In Fig. 8c, MUSIC obtains separations less than the 49° beamwidth much less frequently than MLE, in about 10% of $N > 1$ solutions, as compared with 69% for MLE. Resolution as defined by (6) represents a significant difference between the DOA and detection methods. These results also demonstrate that both MUSIC and MLE are able to resolve separations of less than the antenna beamwidths.

A substantial fraction of MLE-LR DOA solutions have a separation of less than 10° in Figs. 8b and 8d, with the SeaSonde producing about 23% and the RA8 about 44%. One possible interpretation is that these $N > 1$, small separations result from the inherent uncertainty of the DOA-detection calculations, and that the LR method fails to distinguish between, for example, the difference between a covariance matrix constructed from a particular $N = 1$ solution, or a covariance matrix constructed from $N = 2$ closely spaced signal sources. An alternative interpretation is that the (e.g.) $N = 2$ solutions are a better fit to the data than the $N = 1$, because the data result from ocean current structures that span several degrees. Typically, ocean current structures resolved by HF radar span several kilometers, and inspection of the radial data for these sites suggests that the spatial extent of current structures are much larger than length scales suggested by <10° separations in bearing. The results in Fig. 8 may indicate an important difference between the DOA–detection methods. However, these results contrast with the overall result suggested by the synthetic radial and drifter comparisons (Figs. 4 and 5), which is that the best comparisons were found with the most

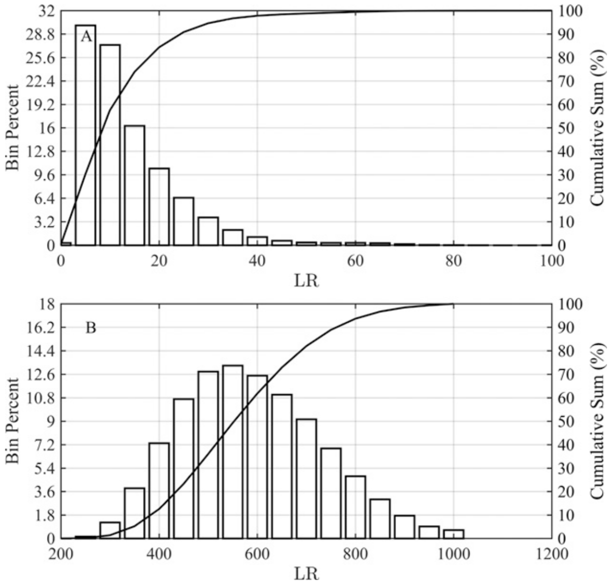

FIG. 9. Histograms of all LR values computed for (a) the SeaSonde at COP1 and (b) the UH-HFDR RA-8 array at LPWR.

selective detection parameters, resulting in the most $N = 1$ solutions.

c. Threshold recommendations

Figure 9 shows histograms of all LR values computed for HF radars at COP and LPWR, with the histograms conforming to the expectation of a χ^2 distribution (Ottersten et al. 1993). Figure 9a illustrates that the range of LR thresholds for the SeaSonde at COP (between 10 and 70) represent the 55th to 100th percentile for the cumulative sum. Similarly, Fig. 9b shows that the LR thresholds used (400–800) for LPWR represent the 15th to 95th percentiles on the cumulative sum. As stated above, the PDFs (approximated in the figure) are a function of K and M, such that radars with similar processing parameters should obtain similar PDFs. Furthermore, the thresholds used here (e.g., 70 for SeaSondes, 800 for the RA-8 systems, Table 4) to generate Figs. 3 and 6 should produce similar detection results, and that for SeaSondes LR = 35 would produce similar results to MUSIC with the [40 20 2] MUSIC–parameter set. Users of systems with different processing parameters may determine a useful threshold range by first generating the PDF and selecting the LR values at any of the percentiles such as described above.

5. Conclusions

In this paper we describe and test the likelihood ratio for use with the MLE DOA method, constructing a viable method from several suggested possibilities from within the literature. We apply the GLRT philosophy to the problem of determining the number of signal sources N through the sequential calculation of the LR, following Chandran (2006), while using a combination of methods to compute LR values (Swindlehurst and Stoica 1998; Abramovich and Spencer 2004; Abramovich et al. 2009). For SeaSonde ocean surface current HF radars, our results find similar performance in terms of accuracy and coverage when using MLE-LR as when using MUSIC with MUSIC parameter tests developed for the SeaSonde. We also find similar performance for the 8-channel, UH-HFDR systems, operated with an 8-element rectangular receive array (RA-8), when using MUSIC for DOA and MUSIC-Highest for detection as described by Kirincich et al. (2019). Analysis of the separation in bearing between DOA estimates from the same covariance matrix confirms that MLE is not limited in distinguishing closely spaced signal source areas, which may have implications for resolving ocean current structures at scales below previously determined resolutions. Comparisons between measurements, however, suggests best results are found with parameters selecting for more single-bearing solutions (low N in this paper). A further result of this study is that improvement in radial velocity accuracy can be obtained for SeaSonde operators by setting the SeaSonde detection parameters to the lower of the manufacturer recommended settings, [10 5 8]. This setting produced about 97% single-bearing solutions, with the accuracy coming at the expense of a decrease in the number of radial observations.

Given the recommendations for threshold number given above, use of MLE-LR represents a viable alternative to MUSIC-based direction-finding methods and has the particular benefit of detecting more closely spaced signals then is possible for MUSIC. The present work completes the development of MLE as a direction-finding method for HFR surface current mapping use, by presenting a robust and vetted detection method that does not suffer from the limitations of approaches based on the eigendecomposition of the data covariance matrix. An online software repository contains the code used in this paper, which is generalized to work with arbitrary receive arrays or DOA methods (Emery 2021).

TABLE 4. Recommended LR thresholds for the number of data snapshots K and receive antenna elements M used here.

Dataset	LR threshold	K	M
SeaSondes	70	6	3
UH-HFDR	800	8	8

Acknowledgments. This work was supported by the National Science Foundation (NSF) under Grant OCE-1658475. Computing resources were provided by the UCSB Center for Scientific Computing through an NSF MRSEC (DMR-1720256) and NSF CNS-1725797. Any opinions, findings, and conclusions or recommendations expressed in this material are those of the authors and do not necessarily reflect the views of the National Science Foundation.

Data availability statement. All data created or used during this study are openly available online (https://doi.org/10.21424/R4RH08).

REFERENCES

Abramovich, Y., and N. Spencer, 2004: Performance breakdown of subspace-based methods in arbitrary antenna arrays: GLRT-based prediction and cure. *2004 IEEE Int. Conf. on Acoustics, Speech, and Signal Processing*, Montreal, QC, Canada, IEEE, https://doi.org/10.1109/ICASSP.2004.1326208.

——, B. A. Johnson, and X. Mestre, 2009: DOA estimation in the small-sample threshold region. *Classical and Modern Direction-of-Arrival Estimation*, T. E. Tuncer and B. Friedlander, Eds., Academic Press, 219–287, https://doi.org/10.1016/B978-0-12-374524-8.00006-4.

Amar, A., and A. J. Weiss, 2007: Resolution of closely spaced deterministic with given success rate signals. 2007 *IEEE Int. Symp. on Information Theory*, Nice, France, IEEE, 1791–1795, https://doi.org/10.1109/ISIT.2007.4557481.

Barrick, D. E., and B. J. Lipa, 1999: Radar angle determination with MUSIC direction finding. U.S. Patent 5 990 834, 12 pp.

Chandran, S., 2006: *Advances in Direction-of-Arrival Estimation.* Artech House, 474 pp.

Cosoli, S., A. Mazzoldi, and M. Gačić, 2010: Validation of surface current measurements in the northern Adriatic Sea from high-frequency radars. *J. Atmos. Oceanic Technol.*, **27**, 908–919, https://doi.org/10.1175/2009JTECHO680.1.

Davis, R. E., 1985: Drifter observations of coastal surface currents during CODE: The statistical and dynamical views. *J. Geophys. Res.*, **90**, 4756–4772, https://doi.org/10.1029/JC090iC03p04756.

de Paolo, T., T. Cook, and E. Terrill, 2007: Properties of HF radar compact antenna arrays and their effect on the MUSIC algorithm. *OCEANS 2007*, Vancouver, BC, Canada, IEEE, https://doi.org/10.1109/OCEANS.2007.4449265.

Emery, B. M., 2020: Evaluation of alternative direction of arrival methods for oceanographic HF radars. *IEEE J. Oceanic Eng.*, **45**, 990–1003, https://doi.org/10.1109/JOE.2019.2914537.

——, 2021: HFR CS processing toolbox for MATLAB, software release version 2.0. Zenodo, https://doi.org/10.5281/zenodo.5598294.

——, and L. Washburn, 2019: Uncertainty estimates for SeaSonde HF radar ocean current observations. *J. Atmos. Oceanic Technol.*, **36**, 231–247, https://doi.org/10.1175/JTECH-D-18-0104.1.

——, ——, and J. Harlan, 2004: Evaluating radial current measurements from CODAR high-frequency radars with moored current meters. *J. Atmos. Oceanic Technol.*, **21**, 1259–1271, https://doi.org/10.1175/1520-0426(2004)021<1259:ERCMFC>2.0.CO;2.

Graber, H. C., B. K. Haus, R. D. Chapman, and L. K. Shay, 1997: HF radar comparisons with moored estimates of current speed and direction: Expected differences and implications. *J. Geophys. Res.*, **102**, 18 749–18 766, https://doi.org/10.1029/97JC01190.

Kaplan, D., M. Cook, and D. Atwater, 2007: HFRProgs: High frequency radar program suite. GitHub, https://github.com/rowg/hfrprogs.

Kelly, E. J., and K. M. Forsythe, 1989: Adaptive detection and parameter estimation for multidimensional signal models. MIT Lexington Lincoln Lab Tech. Rep., 241 pp.

Kirincich, A., 2016: Remote sensing of the surface wind field over the coastal ocean via direct calibration of HF radar backscatter power. *J. Atmos. Oceanic Technol.*, **33**, 1377–1392, https://doi.org/10.1175/JTECH-D-15-0242.1.

——, 2018: LERA HF radar developer package. GitHub, https://github.com/akirincich/lera_dpd.git.

——, B. Emery, L. Washburn, and P. Flament, 2019: Improving surface current resolution using direction finding algorithms for multiantenna high-frequency radars. *J. Atmos. Oceanic Technol.*, **36**, 1997–2014, https://doi.org/10.1175/JTECH-D-19-0029.1.

Krim, H., and M. Viberg, 1996: Two decades of array signal processing research: The parametric approach. *IEEE Signal Process. Mag.*, **13**, 67–94, https://doi.org/10.1109/79.526899.

Laws, K. E., D. M. Fernandez, and J. D. Paduan, 2000: Simulation-based evaluations of HF radar ocean current algorithms. *IEEE J. Oceanic Eng.*, **25**, 481–491, https://doi.org/10.1109/48.895355.

Lipa, B. J., 2003: Uncertainties in SeaSonde current velocities. *Proc. IEEE/OES Seventh Working Conf. on Current Measurement Technology*, San Diego, CA, IEEE, 95–100, https://doi.org/10.1109/CCM.2003.1194291.

——, and D. E. Barrick, 1983: Least-squares methods for the extraction of surface currents from CODAR crossed-loop data: Application at ARSLOE. *IEEE J. Oceanic Eng.*, **8**, 226–253, https://doi.org/10.1109/JOE.1983.1145578.

——, B. Nyden, D. S. Ullman, and E. Terrill, 2006: SeaSonde radial velocities: Derivation and internal consistency. *IEEE J. Oceanic Eng.*, **31**, 850–861, https://doi.org/10.1109/JOE.2006.886104.

Liu, Y., R. H. Weisberg, C. R. Merz, S. Lichtenwalner, and G. J. Kirkpatrick, 2010: HF radar performance in a low-energy environment: CODAR SeaSonde experience on the west Florida shelf. *J. Atmos. Oceanic Technol.*, **27**, 1689–1710, https://doi.org/10.1175/2010JTECHO720.1.

Molcard, A., P. Poulain, P. Forget, A. Griffa, Y. Barbin, J. Gaggelli, J. De Maistre, and M. Rixen, 2009: Comparison between VHF radar observations and data from drifter clusters in the Gulf of La Spezia (Mediterranean Sea). *J. Mar. Syst.*, **78**, S79–S89, https://doi.org/10.1016/j.jmarsys.2009.01.012.

Ohlmann, C., P. White, L. Washburn, B. Emery, E. Terrill, and M. Otero, 2007: Interpretation of coastal HF radar–derived surface currents with high-resolution drifter data. *J. Atmos. Oceanic Technol.*, **24**, 666–680, https://doi.org/10.1175/JTECH1998.1.

Ottersten, B., M. Viberg, P. Stoica, and A. Nehorai, 1993: Exact and large sample ML techniques for parameter estimation and detection in array processing. *Radar Array Processing*, Springer, 99–151.

Paduan, J. D., K. C. Kim, M. S. Cook, and F. P. Chavez, 2006: Calibration and validation of direction-finding high-frequency radar ocean surface current observations. *IEEE J. Oceanic Eng.*, **31**, 862–875, https://doi.org/10.1109/JOE.2006.886195.

Percival, D. B., and A. T. Walden, 1993: *Spectral Analysis for Physical Applications.* Cambridge University Press, 583 pp.

Schmidt, R., 1986: Multiple emitter location and signal parameter estimation. *IEEE Trans. Antennas Propag.*, **34**, 276–280, https://doi.org/10.1109/TAP.1986.1143830.

Stewart, R. H., and J. W. Joy, 1974: HF radio measurements of ocean surface currents. *Deep-Sea Res. Oceanogr. Abstr.*, **21**, 1039–1049, https://doi.org/10.1016/0011-7471(74)90066-7.

Swindlehurst, A. L., and P. Stoica, 1998: Maximum likelihood methods in radar array signal processing. *Proc. IEEE*, **86**, 421–441, https://doi.org/10.1109/5.659495.

Tuncer, T. E., T. K. Yasar, and B. Friedlander, 2009: Narrowband and wideband DOA estimation for uniform and nonuniform linear arrays. *Classical and Modern Direction-of-Arrival Estimation*, E. Tuncer and B. Friedlander, Eds., Elsevier, 125–159.

Van Trees, H. L., 2002: *Optimum Array Processing*. Part IV, *Detection, Estimation and Modulation Theory*, John Wiley and Sons, 1472 pp., https://doi.org/10.1002/0471221104.

Wax, M., 1991: Detection and localization of multiple sources via the stochastic signals model. *IEEE Trans. Signal Process.*, **39**, 2450–2456, https://doi.org/10.1109/78.98000.

——, and T. Kailath, 1985: Detection of signals by information theoretic criteria. *IEEE Acoust. Speech Signal Process.*, **33**, 387–392, https://doi.org/10.1109/TASSP.1985.1164557.

Wilks, S. S., 1938: The large-sample distribution of the likelihood ratio for testing composite hypotheses. *Ann. Math. Stat.*, **9**, 60–62, https://doi.org/10.1214/aoms/1177732360.

Wyatt, L. R., J. J. Green, A. Middleditch, M. D. Moorhead, J. Howarth, M. Holt, and S. Keogh, 2006: Operational wave, current, and wind measurements with the Pisces HF radar. *IEEE J. Oceanic Eng.*, **31**, 819–834, https://doi.org/10.1109/JOE.2006.888378.

Ziskind, I., and M. Wax, 1988: Maximum likelihood localization of multiple sources by alternating projection. *IEEE Trans. Acoust. Speech Signal Process.*, **36**, 1553–1560, https://doi.org/10.1109/29.7543.